Int. J. Therm. Sci. (2001) 40, 94–103

S1290-0729(00)00274-X/FLA

Modelling of engine in-cylinder thermodynamics under high values of ignition retard

Siew Hwa Chan, J. Zhu

School of Mechanical and Production Engineering, Nanyang Technological University, Singapore

(Received 29 November 1999, accepted 26 January 2000)

Abstract — This paper presents the work on a carburetted gasoline engine, in particular the complete modelling of an engine in-cylinder thermodynamics under high values of ignition retard (HVIR). The "combustion" is a two-zone burnt/unburned model with the fuel burning rate described by a Wiebe function. Under extreme spark timing retard conditions, the Wiebe function describing the heat release of the fuel–air reactions was modified to account for the critical change in pressure distribution in the cylinder due to the abnormal spark retard. An empirical correlation for cylinder pressure variation during the mass blowdown process, which occurs between the exhaust valve opened and bottom-dead-centre, was included in the simulation to enhance the predictive capability of the engine model. The complicated mass blowdown process across the exhaust valves was simplified by two processes: (i) isentropic expansion from the cylinder pressure to the constant exhaust manifold pressure, and (ii) constant pressure throttling which gives rise to increased exhaust gas temperature due to the recovery of kinetic energy. © 2001 Éditions scientifiques et médicales Elsevier SAS

engine thermodynamics / high values of ignition retard / modified Wiebe function / mass blowdown

Nomenclature

A	area exposed to heat transfer	m^2
b	cylinder bore	m
BDC	bottom dead centre (180 °CA)	
cm	piston mean speed	$m{\cdot}s^{-1}$
c_p	specific heat at constant pressure	$kJ{\cdot}kg^{-1}{\cdot}K^{-1}$
C_b	blowby coefficient	s^{-1}
E	total energy	kJ
h	specific enthalpy	$kJ{\cdot}kg^{-1}$
	or heat transfer coefficient	$W{\cdot}m^{-2}{\cdot}K^{-1}$
HVIR	high values of ignition retard	
KE	kinetic energy	kJ
l	connecting rod length	m
m	mass	kg
n	number	
p	pressure	kPa
Q	heat transfer	kJ
r	compression ratio	
s	specific entropy	$kJ{\cdot}kg^{-1}{\cdot}K^{-1}$
S	stroke length	m
t	time	s
T	temperature	K
u	specific internal energy	$kJ{\cdot}kg^{-1}$
	or exhaust gas velocity	$m{\cdot}s^{-1}$
U	internal energy	kJ
v	specific volume	$m^3{\cdot}kg^{-1}$
	or kinematic viscosity	$m^2{\cdot}s^{-1}$
V	volume	m^3
W	work done	kJ
x	burnt mass fraction	
ε	$= S/2l$	
γ	ratio of specific heats	
θ	crank angle	°CA
θ_b	combustion duration	°CA
θ_{ig}	ignition timing $= \theta_s - \theta_d$	
θ_s	spark timing	°CA
θ_d	ignition delay	°CA
ω	angular velocity	$rad{\cdot}s^{-1}$
Ω	engine speed	min^{-1}

Subscripts

amb	ambient
b	burnt gas
c	clearance
cyl	cylinder
EVO	exhaust valve opened
g	gas

E-mail address: mshchan@ntu.edu.sg (S.H. Chan).

i	intake
IVC	intake valve closure
j	component index
l	blowby
res	residual gas
u	unburned gas
w	wall

1. INTRODUCTION

Previous studies revealed that proper engine management, in particular by implementing the high values of ignition retard (HVIR) control can rapidly light-off the three-way catalyst (TWC) and hence largely reduce the carbon monoxide (CO), unburned hydrocarbon (uHC) and oxides of nitrogen (NO_x) in the cold-start phase [1]. Similar approach has been reported by Ashley [2] and Heywood [3] as one of the promising techniques for future cold-start phase engine emissions control. A detailed literature review for cold-start phase engine emissions control strategies can be found in [1].

In the HVIR control, spark timing, idling speed, and air–fuel ratio are all monitored and controlled by a microprocessor. The exhaust gas energy at exhaust valves opened (EVO) associated with HVIR control has been substantially improved due to the increase in both exhaust gas temperature and mass flow rate. This improvement, however, is at the expense of engine performance and is tolerable only for a short period of HVIR implementation (about 30 s) at tuned idling speed. The advantages of increased enthalpy level in the exhaust gas at EVO include (i) to promote post-flame reactions and (ii) to shorten catalyst's warm up time. Proper spark timing control is crucial as excessive retard causing engine backfiring, while insufficient retard of spark timing causing increased engine-out emissions.

This paper presents the work on modelling of in-cylinder thermodynamics under HVIR, in particular the effect of spark retard on cylinder pressure distribution. An engine simulation program was developed based on filling-and-emptying technique, and the "combustion" is essentially a two-zone burnt/unburned model with the fuel burning rate described by a Wiebe function. Under extreme spark timing retard conditions, the Wiebe function describing the heat release of the fuel–air reactions was modified to account for the critical change in pressure distribution in the cylinder due to the abnormal spark retard. In addition to the modified Wiebe function, an empirical correlation for cylinder pressure variation during the mass blowdown process, which occurs between the exhaust valve opened and bottom-dead-centre, was included in the simulation to enhance the predictive capability of the engine model. The complicated mass blowdown process across the exhaust valves was simplified by two processes: (i) isentropic expansion from the cylinder pressure to the constant exhaust manifold pressure, and (ii) constant pressure throttling which gives rise to increased exhaust gas temperature due to the recovery of kinetic energy.

The current work is limited to engine warmed up conditions, and the results validation, in particular, the cylinder pressure are based on steady-speed experimental data.

2. ENGINE MODEL

A zero-dimensional thermodynamic cycle simulation with two-zone burnt/unburned combustion model, mainly based on Ferguson's [4] work, was developed to predict the cylinder pressure, burnt and unburned temperatures of gases, work done, heat loss, enthalpy of exhaust gas, mass flow rate, etc. The zero-dimensional model is based on the first law of thermodynamics in which an empirical relationship between the fuel burning rate and crank angle position is established. The two-zone combustion model assumes that at any instant of time during the combustion, the cylinder volume is divided into burnt and unburned zones by an infinitesimally thin flame front. Each zone is assumed to be in thermodynamic equilibrium and both zones having the same uniform pressure at any instant of time.

The region in the combustion chamber is treated as a control volume as illustrated in *figure 1*. The governing equations are the mass and energy conservation equations and equations of state. These equations, with crank angle as the independent variable, form the building block of this thermodynamic model.

2.1. Mass and energy balances

For a control volume enclosing the fuel–air mixture, the rate of change of total mass of an open system is equal to the sum of mass flowing into and out of the system:

$$\dot{m} = \sum_j \dot{m}_j \tag{1}$$

Applying the first law of thermodynamics to an open thermodynamic system, the energy equation is

$$\dot{E} = \dot{Q} - \dot{W} + \sum_j \dot{m}_j h_j \tag{2}$$

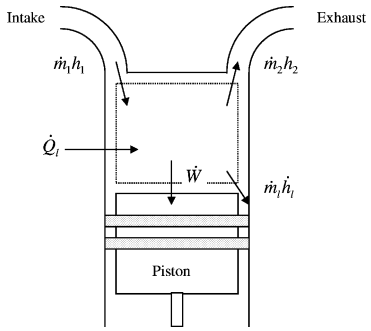

Figure 1. Schematic of combustion chamber as an open thermodynamic system.

Prescribing the conservation of mass and energy equations as functions of crank angle, equations (1) and (2) become

$$\frac{\mathrm{d}m}{\mathrm{d}\theta} = \sum_j \frac{\mathrm{d}m_j}{\mathrm{d}\theta} \tag{3}$$

$$\frac{\mathrm{d}(mu)}{\mathrm{d}\theta} = \frac{\mathrm{d}Q}{\mathrm{d}\theta} - p\frac{\mathrm{d}V}{\mathrm{d}\theta} + \sum_j h_j \frac{\mathrm{d}\dot{m}_j}{\mathrm{d}\theta} \tag{4}$$

The latter neglects the changes of kinetic energy and potential energy in the control volume.

2.2. Thermal properties

In a two-zone burnt/unburned model, the unburned mixture and burnt mixture zones are each treated as separate open systems. Hence, the specific internal energy and volume are given by

$$u = \frac{U}{m} = x u_\mathrm{b} + (1-x)u_\mathrm{u} \tag{5}$$

$$v = \frac{V}{m} = x v_\mathrm{b} + (1-x)v_\mathrm{u} \tag{6}$$

Assuming that the pressures of burnt and unburned gases are equal, v_b and v_u are functions of both T_b, T_u and p. Hence,

$$\frac{\mathrm{d}v_\mathrm{b}}{\mathrm{d}\theta} = \frac{\partial v_\mathrm{b}}{\partial T_\mathrm{b}}\frac{\mathrm{d}T_\mathrm{b}}{\mathrm{d}\theta} + \frac{\partial v_\mathrm{b}}{\partial p}\frac{\mathrm{d}p}{\mathrm{d}\theta} \tag{7}$$

$$\frac{\mathrm{d}v_\mathrm{u}}{\mathrm{d}\theta} = \frac{\partial v_\mathrm{u}}{\partial T_\mathrm{u}}\frac{\mathrm{d}T_\mathrm{u}}{\mathrm{d}\theta} + \frac{\partial v_\mathrm{u}}{\partial p}\frac{\mathrm{d}p}{\mathrm{d}\theta} \tag{8}$$

The thermodynamic properties of a complex chemical equilibrium composition existing in any fuel–air reaction are obtained using the method proposed by Olikara and Borman [5] which is an equilibrium constants based method for solving chemical equilibrium compositions, specific heats, internal energies, enthalpies, entropies, and other partial derivatives useful in thermodynamic analysis.

By substituting logarithmic derivatives obtained from Olikara and Borman's method, equations (7) and (8) can be rewritten as

$$\frac{\mathrm{d}v_\mathrm{b}}{\mathrm{d}\theta} = \frac{v_\mathrm{b}}{T_\mathrm{b}}\frac{\partial \ln v_\mathrm{b}}{\partial \ln T_\mathrm{b}}\frac{\mathrm{d}T_\mathrm{b}}{\mathrm{d}\theta} + \frac{v_\mathrm{b}}{p}\frac{\partial \ln v_\mathrm{b}}{\partial \ln p}\frac{\mathrm{d}p}{\mathrm{d}\theta} \tag{9}$$

$$\frac{\mathrm{d}v_\mathrm{u}}{\mathrm{d}\theta} = \frac{v_\mathrm{u}}{T_\mathrm{u}}\frac{\partial \ln v_\mathrm{u}}{\partial \ln T_\mathrm{u}}\frac{\mathrm{d}T_\mathrm{u}}{\mathrm{d}\theta} + \frac{v_\mathrm{u}}{p}\frac{\partial \ln v_\mathrm{u}}{\partial \ln p}\frac{\mathrm{d}p}{\mathrm{d}\theta} \tag{10}$$

Likewise, the internal energies of both the burnt and unburned gases with same pressure condition are

$$\frac{\mathrm{d}u_\mathrm{b}}{\mathrm{d}\theta} = \frac{\partial u_\mathrm{b}}{\partial T_\mathrm{b}}\frac{\mathrm{d}T_\mathrm{b}}{\mathrm{d}\theta} + \frac{\partial u_\mathrm{b}}{\partial p}\frac{\mathrm{d}p}{\mathrm{d}\theta} \tag{11}$$

$$\frac{\mathrm{d}u_\mathrm{u}}{\mathrm{d}\theta} = \frac{\partial u_\mathrm{u}}{\partial T_\mathrm{u}}\frac{\mathrm{d}T_\mathrm{u}}{\mathrm{d}\theta} + \frac{\partial u_\mathrm{u}}{\partial p}\frac{\mathrm{d}p}{\mathrm{d}\theta} \tag{12}$$

The above can be rewritten to include the logarithmic terms (4) as

$$\frac{\mathrm{d}u_\mathrm{b}}{\mathrm{d}\theta} = \left(c_{p\,\mathrm{b}} - \frac{p v_\mathrm{b}}{T_\mathrm{b}}\frac{\partial \ln v_\mathrm{b}}{\partial \ln T_\mathrm{b}}\right)\frac{\mathrm{d}T_\mathrm{b}}{\mathrm{d}\theta} - v_\mathrm{b}\left(\frac{\partial \ln v_\mathrm{b}}{\partial \ln T_\mathrm{b}} + \frac{\partial \ln v_\mathrm{b}}{\partial \ln p}\right)\frac{\mathrm{d}p}{\mathrm{d}\theta} \tag{13}$$

$$\frac{\mathrm{d}u_\mathrm{u}}{\mathrm{d}\theta} = \left(c_{p\,\mathrm{u}} - \frac{p v_\mathrm{u}}{T_\mathrm{u}}\frac{\partial \ln v_\mathrm{u}}{\partial \ln T_\mathrm{u}}\right)\frac{\mathrm{d}T_\mathrm{u}}{\mathrm{d}\theta} - v_\mathrm{u}\left(\frac{\partial \ln v_\mathrm{u}}{\partial \ln T_\mathrm{u}} + \frac{\partial \ln v_\mathrm{u}}{\partial \ln p}\right)\frac{\mathrm{d}p}{\mathrm{d}\theta} \tag{14}$$

2.3. Trapped mass in control volume

The trapped mass in the control volume at various periods is given by

$$m = \frac{V(\theta)}{v_\mathrm{u}} \quad \text{when } \theta_\mathrm{IVC} \geq \theta > -360\,^\circ\mathrm{CA} \text{ (intake)} \tag{15a}$$

$$m = m_\mathrm{IVC}\,\mathrm{e}^{-C_\mathrm{b}(\theta-\theta_\mathrm{IVC})/\omega}$$

$$\text{when } \theta_\mathrm{EVO} \geq \theta > \theta_\mathrm{IVC} \text{ (valve-closed)} \tag{15b}$$

$$m = \frac{V(\theta)}{v_\mathrm{b}} \quad \text{when } 360\,^\circ\mathrm{CA} \geq \theta > \theta_\mathrm{EVO}$$

$$\text{(blowdown and exhaust)} \tag{15c}$$

The cylinder volume at any crank angle is given by

$$V(\theta) = V_\mathrm{c}\left\{1 + \frac{r-1}{2}\left\{1 - \cos\theta + \frac{1}{\varepsilon}\left[1 - \left(1 - \varepsilon^2 \sin^2\theta\right)^{1/2}\right]\right\}\right\} \tag{16}$$

2.4. Fuel burning rate correlation

The fuel burning rate in the SI engine is normally modelled by the Wiebe function [6], however, it is modified in this study to include the effect of HVIR on the heat release pattern. The burnt mass fraction is given by

$$x(\theta) = 1 - \exp\left[-a\left(\frac{\theta - \theta_{\mathrm{ig}}}{\theta_{\mathrm{b}}}\right)^{m+1}\right] \tag{17}$$

where the efficiency parameter is $a = 5$ and the shape factor is $m = 1.5$ for the engine used in this study.

2.5. Heat transfer from gases to cylinder wall

Heat transfer into a thermodynamic system is expressed in terms of the heat loss:

$$\frac{\mathrm{d}Q}{\mathrm{d}\theta} = \frac{-\dot{Q}_{\mathrm{l}}}{\omega} = \frac{-\dot{Q}_{\mathrm{b}} - \dot{Q}_{\mathrm{u}}}{\omega} \tag{18}$$

where

$$\dot{Q}_{\mathrm{b}} = h \sum_{i=\mathrm{h,p,l}} A_{\mathrm{b}i}(T_{\mathrm{b}} - T_{\mathrm{w}i}) \tag{19}$$

$$\dot{Q}_{\mathrm{u}} = h \sum_{i=\mathrm{h,p,l}} A_{\mathrm{u}i}(T_{\mathrm{u}} - T_{\mathrm{w}i}) \tag{20}$$

wherein $A_{\mathrm{b}i}$ and $A_{\mathrm{u}i}$ are the areas of burnt and unburned gases in contact with each combustion chamber component at temperature $T_{\mathrm{w}i}$, and subscripts h, p, l refer to cylinder head, piston crown and liner, respectively. The instantaneous heat transfer coefficient (h) adopted from Woschni [7] is given by

$$h = 0.82 b^{-0.2}\left(p \cdot 10^{-3} \cdot c\right)^{0.8} T^{-0.53} \tag{21}$$

where

$$c = 6.18 cm \quad \text{(for gas exchange process)} \tag{22}$$

$$c = 2.28 cm + 0.00324 T \frac{\Delta p}{p_{\mathrm{IVC}}} \frac{V}{V_{\mathrm{IVC}}} \quad \text{(for other processes)} \tag{23}$$

$$T = x T_{\mathrm{b}} + (1 - x) T_{\mathrm{u}} \tag{24}$$

$$A_{\mathrm{b}i} = A_i x^{1/2} \tag{25}$$

$$A_{\mathrm{u}i} = A_i\left(1 - x^{1/2}\right) \tag{26}$$

and Δp is the instantaneous pressure difference between the firing engine and motoring engine at the same crank angle. The latter is estimated by using the isentropic relation $pV^{\gamma} = p_{\mathrm{IVC}} V_{\mathrm{IVC}}^{\gamma}$. The surface areas in contact with hot gases can be expressed by

$$A_{\mathrm{h}} = \frac{\pi b^2}{2} \quad \text{(hemispheric cylinder head)}$$

$$A_{\mathrm{p}} = \frac{\pi b^2}{4} \quad \text{(flat piston crown)}$$

$$A_{\mathrm{l}} = \frac{4V(\theta)}{b} \quad \text{(liner surface area exposed to gases)}$$

Equations (25) and (26) assume that the fraction of cylinder area exposed to burnt gas is proportional to the square root of the burnt mass fraction which reflects the fact that burnt gas occupies a larger volume fraction than the unburned gas [4].

2.6. Blowby energy loss

The enthalpy loss due to blowby is expressed as

$$h_{\mathrm{l}} = \left(1 - x^2\right) h_{\mathrm{u}} + x^2 h_{\mathrm{b}} \tag{27}$$

which implicitly indicates that more leaking is due to the unburned gas compared with the burnt gas in the early stage of combustion.

2.7. Governing equations

Differentiating the specific volume (equation (6)) with respect to crank angle and incorporating equations (9) and (10) yields

$$\begin{aligned}
&\frac{1}{m}\frac{\mathrm{d}V}{\mathrm{d}\theta} + \frac{V C_{\mathrm{b}}}{m\omega} \\
&\quad = x\,\frac{v_{\mathrm{b}}}{T_{\mathrm{b}}}\frac{\partial \ln v_{\mathrm{b}}}{\partial \ln T_{\mathrm{b}}}\frac{\mathrm{d}T_{\mathrm{b}}}{\mathrm{d}\theta} + (1-x)\frac{v_{\mathrm{u}}}{T_{\mathrm{u}}}\frac{\partial \ln v_{\mathrm{u}}}{\partial \ln T_{\mathrm{u}}}\frac{\mathrm{d}T_{\mathrm{u}}}{\mathrm{d}\theta} \\
&\qquad + \left[x\,\frac{v_{\mathrm{b}}}{p}\frac{\partial \ln v_{\mathrm{b}}}{\partial \ln p} + (1-x)\frac{v_{\mathrm{u}}}{p}\frac{\partial \ln v_{\mathrm{u}}}{\ln p}\right]\frac{\mathrm{d}p}{\mathrm{d}\theta} \\
&\qquad + (v_{\mathrm{b}} - v_{\mathrm{u}})\frac{\mathrm{d}x}{\mathrm{d}\theta}
\end{aligned} \tag{28}$$

where the blowby coefficient is $C_{\mathrm{b}} = \dot{m}_{\mathrm{l}}/m$ and $\dot{m}_{\mathrm{l}}$ is the leakage due to blowby.

Expressing the heat loss of burnt and unburned gases as a function of the rate of change of specific entropy gives

$$-\dot{Q}_{\mathrm{b}} = m\omega x T_{\mathrm{b}} \frac{\mathrm{d}s_{\mathrm{b}}}{\mathrm{d}\theta} \tag{29}$$

$$-\dot{Q}_{\mathrm{u}} = m\omega (1-x) T_{\mathrm{u}} \frac{\mathrm{d}s_{\mathrm{u}}}{\mathrm{d}\theta} \tag{30}$$

TABLE I
Applicable equations for different processes in an engine cycle

	Intake $-360° \le \theta < \theta_{IVC}$	Compression $\theta_{IVC} \le \theta < \theta_{ig}$	Combustion $\theta_{ig} \le \theta < \theta_{ig} + \theta_b$	Expansion $\theta_{ig} + \theta_b \le \theta < \theta_{EVO}$	Exhaust $-180° \le \theta < 360°$
$\frac{dp}{d\theta}$	0	equation (35)	equation (35)	equation (35)	0
$\frac{dT_b}{d\theta}$	N.A.	N.A.	equation (36)	equation (36)	equation (36)
$\frac{dT_u}{d\theta}$	equation (37)	equation (37)	equation (37)	N.A.	N.A.
f_1	N.A.	equation (38)	equation (38)	equation (38)	N.A.
f_2	N.A.	equation (39)	equation (39)	equation (39)	N.A.
f_3	N.A.	0	equation (40)	0	N.A.
f_4	N.A.	0	equation (41)	equation (41)	N.A.
f_5	N.A.	equation (42)	equation (42)	0	N.A.

where

$$\frac{ds_b}{d\theta} = \left(\frac{c_{pb}}{T_b}\right)\frac{dT_b}{d\theta} - \frac{v_b}{T_b}\frac{\partial \ln v_b}{\partial \ln T_b}\frac{dp}{d\theta} \tag{31}$$

$$\frac{ds_u}{d\theta} = \left(\frac{c_{pu}}{T_u}\right)\frac{dT_u}{d\theta} - \frac{v_u}{T_u}\frac{\partial \ln v_u}{\partial \ln T_u}\frac{dp}{d\theta} \tag{32}$$

Combining equations (19)–(20), (25)–(26), (29)–(30) and (31)–(32), $ds_b/d\theta$ and $ds_u/d\theta$ terms are eliminated. Hence,

$$c_{pb}\frac{dT_b}{d\theta} - v_b\frac{\partial \ln v_b}{\partial \ln T_b}\frac{dp}{d\theta} = \frac{-h\sum_{i=h,p,l} A_{bi}(T_b - T_{wi})}{m\omega x} \tag{33}$$

$$c_{pu}\frac{dT_u}{d\theta} - v_u\frac{\partial \ln v_u}{\partial \ln T_u}\frac{dp}{d\theta} = \frac{-h\sum_{i=h,p,l} A_{ui}(T_u - T_{wi})}{m\omega(1-x)} \tag{34}$$

In addition to equations (28), (33)–(34), differentiating equations (16)–(17) and incorporating these with equations (3), (5)–(6), (9)–(10), (13)–(14) and (18)–(27) into the energy equation, equation (4), the following set of equations is obtained after substantial simplification:

$$\frac{dp}{d\theta} = \frac{f_1 + f_2 + f_3}{f_4 + f_5} \tag{35}$$

$$\frac{dT_b}{d\theta} = \frac{-h\sum_{i=h,p,l} A_{bi}(T_b - T_{wi})}{\omega m c_{pb} x} + \frac{v_b}{c_{pb}}\frac{\partial \ln v_b}{\partial \ln T_b}\frac{dp}{d\theta} + \frac{h_u - h_b}{x c_{pb}}\left[\frac{dx}{d\theta} - (x - x^2)\frac{C_b}{\omega}\right] \tag{36}$$

$$\frac{dT_u}{d\theta} = \frac{-h\sum_{i=h,p,l} A_{ui}(T_u - T_{wi})}{\omega m c_{pu}(1-x)} + \frac{v_u}{c_{pu}}\frac{\partial \ln v_u}{\partial \ln T_u}\frac{dp}{d\theta} \tag{37}$$

where

$$f_1 = \frac{1}{m}\left(\frac{dV}{d\theta} + \frac{VC_b}{\omega}\right) \tag{38}$$

$$f_2 = \frac{h}{\omega m}\left[\frac{v_b}{c_{pb}}\frac{\partial \ln v_b}{\partial \ln T_b}\frac{\sum_{i=h,p,l} A_{bi}(T_b - T_{wi})}{T_b} + \frac{v_u}{c_{pu}}\frac{\partial \ln v_u}{\partial \ln T_u}\frac{\sum_{i=h,p,l} A_{ui}(T_u - T_{wi})}{T_u}\right] \tag{39}$$

$$f_3 = -(v_b - v_u)\frac{dx}{d\theta} - v_b\frac{\partial \ln v_b}{\partial \ln T_b}\frac{h_u - h_b}{c_{pb}T_b}\left[\frac{dx}{d\theta} - \frac{(x - x^2)C_b}{\omega}\right] \tag{40}$$

$$f_4 = x\left[\frac{v_b^2}{c_{pb}T_b}\left(\frac{\partial \ln v_b}{\partial \ln T_b}\right)^2 + \frac{v_b}{p}\frac{\partial \ln v_b}{\partial \ln p}\right] \tag{41}$$

$$f_5 = (1-x)\left[\frac{v_u^2}{c_{pu}T_u}\left(\frac{\partial \ln v_u}{\partial \ln T_u}\right)^2 + \frac{v_u}{p}\frac{\partial \ln v_u}{\partial \ln p}\right] \tag{42}$$

are functions of θ, p, T_b and T_u and their numerical integration can be obtained by using a fifth-order Runge–Kutta method. The application of the above listed equations to different processes in the thermodynamic system is summarised in *table I*.

2.8. Mass blowdown

In addition to the above processes in the previous sections, the mass blowdown process, which occurs between EVO (129 °CA) and BDC (180 °CA), is also considered in this model to enhance the predictive capability of the

model. An empirical correlation for the blowdown pressure is obtained as in the following form:

$$p(\theta) = p_{\mathrm{EVO}} \exp\left[-a\left(\frac{\theta - \theta_{\mathrm{EVO}}}{180^\circ - \theta_{\mathrm{EVO}}}\right)^{m+1}\right] \quad (43)$$

where $a = -\ln(p_{\mathrm{atm}}/p_{\mathrm{EVO}})$ and $m = 0.45$ is the shape factor determined by experimental correlation.

2.9. In-cylinder heat transfer

The heat loss from the hot gas to the engine cooling water through the cylinder head, liner, and piston crown are modelled by heat convection and conduction processes. The convective heat transfer from the gas to the cylinder wall are described by equations (18)–(26), while the conduction of heat across the liner, head, piston is simplified by using a thermal resistance circuit. The thermal inertia of each component is treated as the heat capacitor, which enables one to simulate the thermal loading of the cylinder wall during engine cold start phase. The initial surface temperature of each component exposed to gases is assumed to be identical, and is updated at every engine cycle according to the associated heat transfer mechanism.

2.10. Intake condition

Since the gas dynamic effect is not considered in this study, the cylinder pressure during gas exchange process is assumed constant. This assumption is extended to the calculation of intake pressure (p_{i}) which is assumed to be equal to the manifold pressure.

The residual mass fraction (f), a parameter which is crucial in the determination of the charge air/gas temperature at IVC (T_{i}), is estimated from the previous cycle, i.e.

$$m_{\mathrm{res}} = m(\theta)\big|_{\theta=360^\circ} = (V_{\mathrm{c}}/v_{\mathrm{b}})\big|_{\theta=360^\circ} \quad (44)$$

Hence, the residual mass fraction can be estimated by

$$f = \frac{m_{\mathrm{res}}}{m_{\mathrm{IVC}}} = \frac{V_{\mathrm{c}}}{V_{\mathrm{IVC}}} \frac{v_{\mathrm{u}}|_{\theta=\theta_{\mathrm{IVC}}}}{v_{\mathrm{b}}|_{\theta=360^\circ}} \quad (45)$$

and

$$T_{\mathrm{i}} = (1-f)T_{\mathrm{amb}} + fT_{\mathrm{res}}\left[1 - \left(1 - \frac{p_{\mathrm{i}}}{p_{\mathrm{atm}}}\right)\left(\frac{\gamma - 1}{\gamma}\right)\right] \quad (46)$$

where T_{res} is taken as that at $\theta = 360\,^\circ$CA from the previous cycle.

Equation (46) assumes that the residual gases trapped in the clearance volume were well mixed with the fresh intake charge. Note that the heat absorption by the vaporising fuel droplets and heat transfer between the intake charge and the wall of the intake manifold are negligible and are not considered in this model.

2.11. Cyclic-mean exhaust flow rate and bulk gas temperature

To make provision for the heat transfer calculation along the exhaust system, the cyclic-mean mass flow rate of exhaust gas is considered:

$$\dot{m} = (m_{\mathrm{EVO}} - m_{\mathrm{res}})\frac{\Omega}{120} n_{\mathrm{cyl}} \quad (47)$$

According to Woodward [8, 9], the complicated gas blowdown process between the EVO and BDC across the exhaust valves can be approximated by two simple processes: (i) isentropic expansion from $p(\theta)$ to the constant manifold pressure which is treated as equal to p_{atm}, and (ii) constant pressure throttling which gives rise to the increase in exhaust gas temperature due to the recovery of kinetic energy, i.e.

$$KE(\theta) = \frac{c_p T(\theta)}{\gamma}\left\{1 - (1-\gamma)\frac{p(\theta)}{p_{\mathrm{amb}}} - \gamma\left[\frac{p(\theta)}{p_{\mathrm{amb}}}\right]^{(\gamma-1)/\gamma}\right\} \quad (48)$$

and its associated temperature rise

$$\Delta T_{\mathrm{g}}(\theta) = \frac{KE(\theta)}{c_p} = \frac{T(\theta)}{\gamma}\left\{1 - (1-\gamma)\frac{p(\theta)}{p_{\mathrm{amb}}} - \gamma\left[\frac{p(\theta)}{p_{\mathrm{amb}}}\right]^{(\gamma-1)/\gamma}\right\} \quad (49)$$

Based on Woodward's assumption, the instantaneous exhaust gas temperature at the ports is

$$\begin{aligned} T_{\mathrm{g}}(\theta) &= T(\theta)\left[\frac{p_{\mathrm{amb}}}{p(\theta)}\right]^{(\gamma-1)/\gamma} + \Delta T_{\mathrm{g}}(\theta) \\ &= \frac{T(\theta)}{\gamma}\left\{1 - (1-\gamma)\frac{p(\theta)}{p_{\mathrm{amb}}} + \gamma\left\{\left[\frac{p_{\mathrm{amb}}}{p(\theta)}\right]^{(\gamma-1)/\gamma} - \left[\frac{p(\theta)}{p_{\mathrm{amb}}}\right]^{(\gamma-1)/\gamma}\right\}\right\} \end{aligned} \quad (50)$$

During the exhaust stroke, the gas temperature at exhaust port is assumed to be equal to the gas temperature inside the cylinder which is also varied with the crank angle due to heat transfer between the gas and the walls. Hence, the overall mean gas temperature ($\overline{T}_{\mathrm{g}}$) for the engine cycle is expressed as

$$\overline{T}_{\mathrm{g}} = \frac{\int_{\theta_{\mathrm{EVO}}}^{180^\circ} T_{\mathrm{g}}(\theta) c_p \, \mathrm{d}m(\theta) + \int_{180^\circ}^{360^\circ} T(\theta) c_p \, \mathrm{d}m(\theta)}{c_p (m_{\mathrm{EVO}} - m_{\mathrm{res}})} \quad (51)$$

3. VALIDATION OF PREDICTED CYLINDER PRESSURE

Pressure is, perhaps, the only bulk fundamental parameter that is measurable inside a cylinder of an engine. As cyclic variation is significant during engine warmed up period, in particular for a 3-cylinder Daihatsu engine, 50 cycles of pressure signals were logged down for each test. The ensemble-averaged value of all the 50 cycles' signal was used to validate the predicted results. Note that at 200th cycle after "engine firing" the predicted cylinder pressure results were extracted and compared with the experimental data which are shown in *figures 2–6* covering the spark timings from normal (20 °CA BTDC) to 28 °CA spark retard. The reason for using the 200th cycle is because it corresponds to approximately 15 seconds (engine running at 1 650 rev·min^{-1}) after engine firing, which is the time when the experimental data were collected. Note that the effect of heat transfer on the variation of cylinder pressure/temperature during engine cold start phase is unable to be isolated as the cyclic variabil-

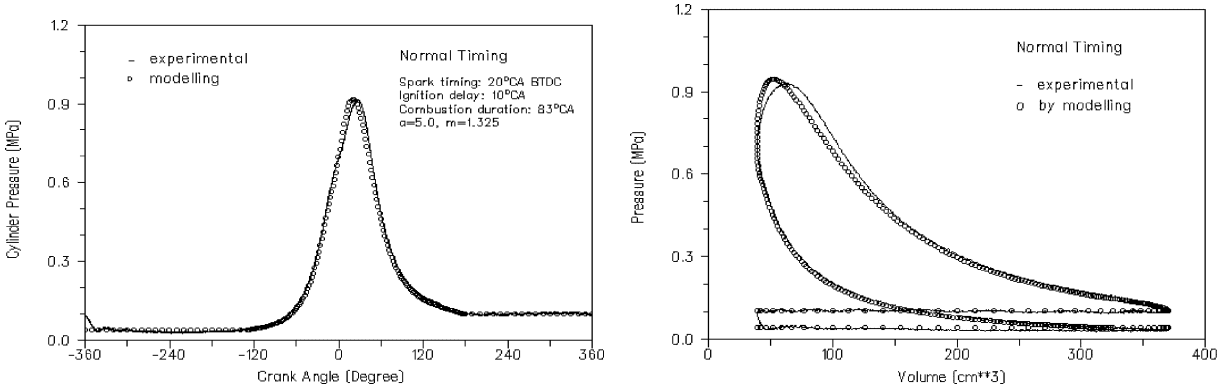

a. b.

Figure 2. Comparison of predicted cylinder pressure with experimental data under normal spark timing condition. a. p–θ diagram. b. p–V diagram.

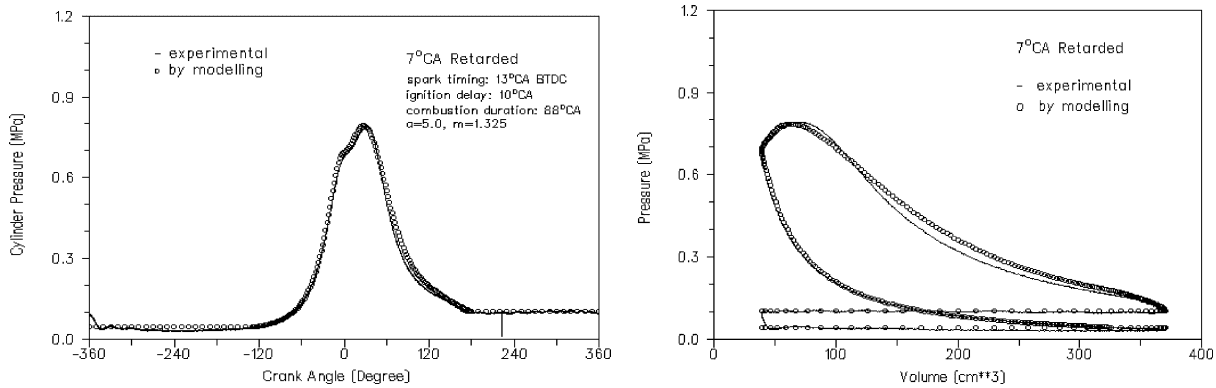

a. b.

Figure 3. Comparison of predicted cylinder pressure with experimental data under 7 °CA spark retard condition. a. p–θ diagram. b. p–V diagram.

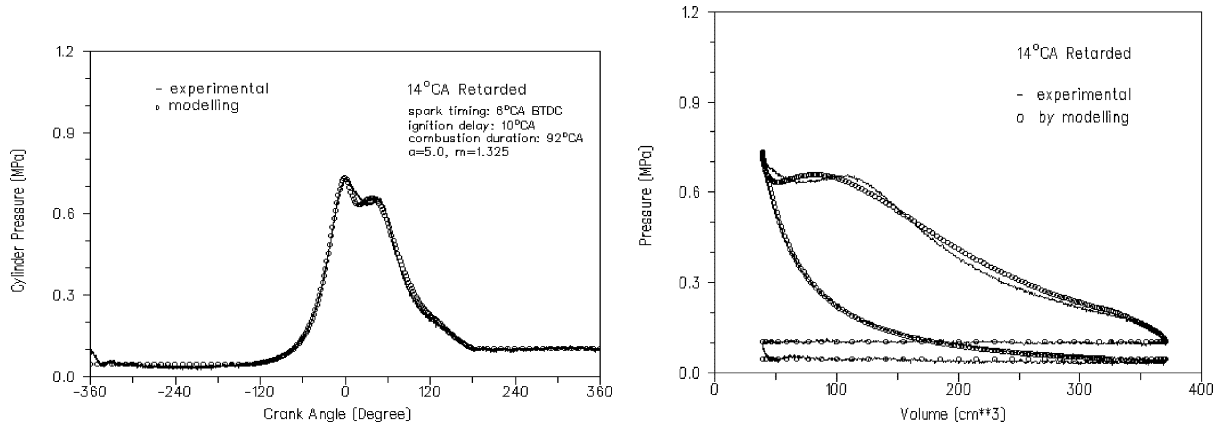

a. b.

Figure 4. Comparison of predicted cylinder pressure with experimental data under 14 °CA spark retard condition. a. p–θ diagram. b. p–V diagram.

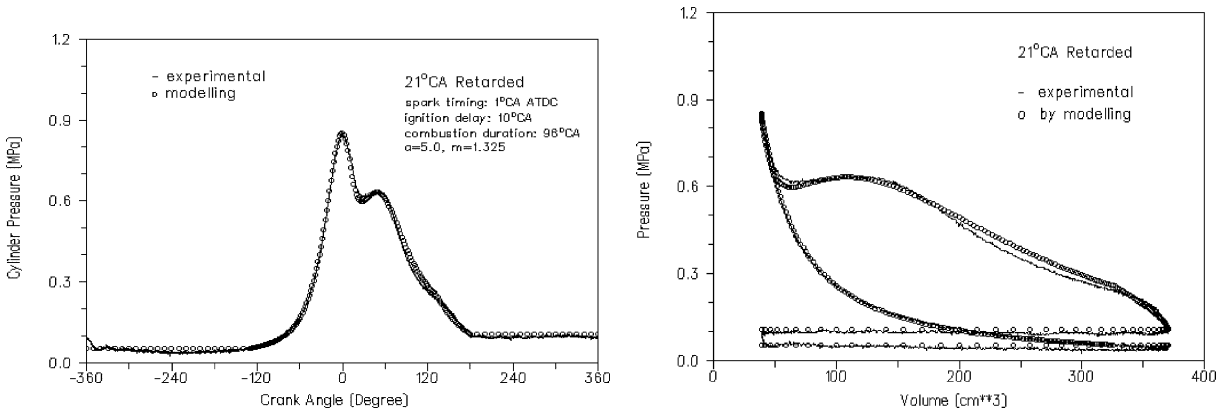

a. b.

Figure 5. Comparison of predicted cylinder pressure with experimental data under 21 °CA spark retard condition. a. p–θ diagram. b. p–V diagram.

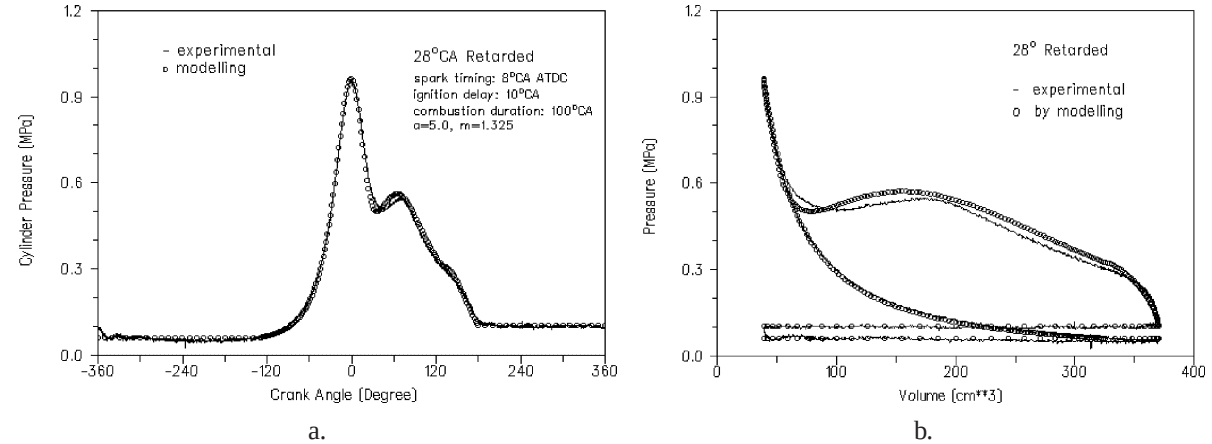

a. b.

Figure 6. Comparison of predicted cylinder pressure with experimental data under 28 °CA spark retard condition. a. p–θ diagram. b. p–V diagram.

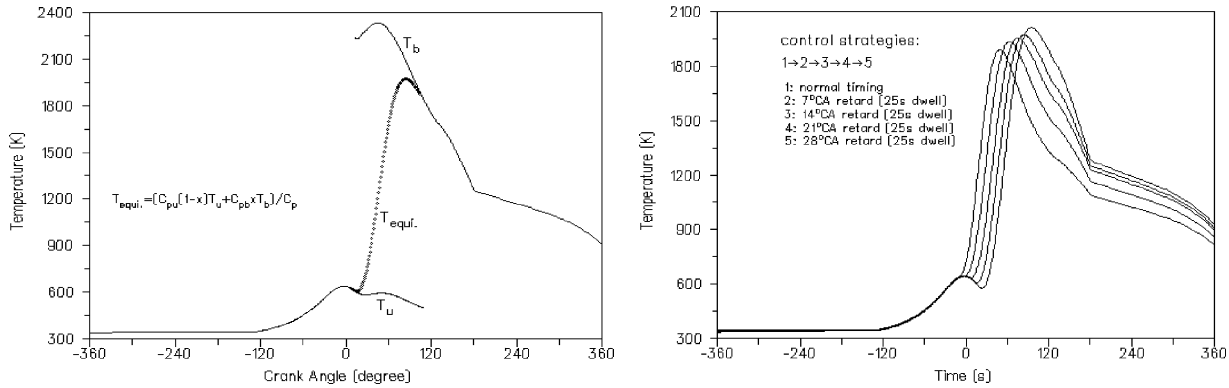

a. b.

Figure 7. a. The equivalent in-cylinder gas temperature derived from burnt and unburned zone temperatures. b. Comparison of in-cylinder gas temperature under varying spark timing conditions.

ity at this phase is of no doubt very complicated, which is governed with the unsteadiness of fuel supply, combustion efficiency, engine oil viscosity, engine control, etc.

Figures 2a–6a show the *p–θ* diagrams while *figures 2b–6b* show the *p–V* diagrams of the engine at tuned idle speed of 1 650 rpm under normal spark timing condition. Validation has shown that the experimental and predicted results are in good agreement. The slight discrepancy may be due to the fact that, in actual engine operation, cycle-to-cycle variation is unavoidable, while in the engine modelling, some empirical correlations based upon the statistical ensemble averaged experimental data were used which are unable to reflect this cycle-to-cycle variation. Another crucial factor is that the model assumes a constant reference pressure during intake process, while the actual manifold pressure fluctuates due to the nature of gas dynamics. A typical single-peak cylinder pressure in the *p–θ* diagram can be seen in the normal timing case, while the twin-peak cylinder pressure evolved as the spark timing retards from the normal timing. The second peak contributes to significant increase in availability of the gas at EVO and it is the intention to make use of this increased thermal energy for heating the TWC to achieve rapid catalyst lightoff at engine cold-start.

4. IN-CYLINDER GAS TEMPERATURE

Figure 7a shows the equivalent in-cylinder gas temperature derived from burnt and unburned zone temperatures under normal timing condition, while *figure 7b* shows the comparison of predicted bulk gas temperature under varying spark timing conditions. Results indicate that the higher the value of spark retard, the higher the peak cylinder temperature will be and hence the higher the exhaust gas temperature at BDC. It can be seen that the gas temperature at EVO (129 °CA) is significantly increased with the increase of the spark retard. At EVO, the gas temperature under normal spark timing condition is well below 1 400 K while for the most of the spark retard cases, the gas temperatures are above 1 400 K for almost the entire period of gas blowdown. Wu and Hochgreb [10] have confirmed that burnt gas temperature at around 1 400 K is critical for in-cylinder post-flame oxidation of uHC leaving the crevice during gas blowdown process. Incorporating with this finding, the simulation results give favourable support to the experimental observation of the improved engine-out uHC emissions under HVIR control as reported in [1].

5. TRAPPED MASS IN CONTROL VOLUME

Figure 8 presents the predicted results of trapped mass in cylinder. It can be seen that, with the increase of the retard value, the mass of gases in the cylinder also increases except for the exhaust stroke, due to the lower gas density associated with higher gas temperature. The increase in trapped mass of gases under spark retard control is attributed to the higher intake pressure caused by widening the throttle in the attempt to maintain the same set engine speed. During the intake process, the mass of gases in the cylinder increases due to the increase in cylinder volume until piston reaches BDC. After that, backflow occurs which causes the decrease of mass until intake

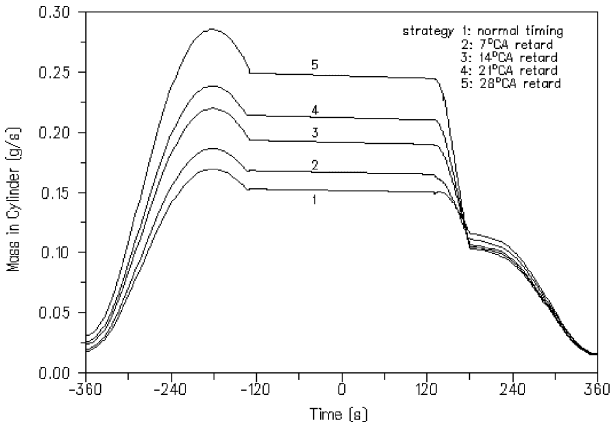

Figure 8. Comparison of in-cylinder trapped mass under different spark timing conditions.

valve closes at −129 °CA. During the valve-closed period from −129 °CA to 129 °CA, the slight decrease in trapped mass is due to the gas blowby as reflected by equation (15b). By the time of EVO, the portion of the cumulative leakage, due to the gas blowby, was suggested to be 2 % for petrol engines [11]. Thus the blowby coefficient C_b during valves-closed period can be determined. For engine operating at 1 650 rpm, the C_b is 0.77.

After EVO, the mass in cylinder decreases sharply as gas blowdown occurs due to the significant pressure difference across the exhaust valve. It can be seen that for the highly retard case, the gas blowdown phenomenon is more prominent. In the most spark retard case, more than 50 % of the exhaust gas exits the exhaust valve during the blowdown process, as compared with the normal timing case, which only accounts for less than 20 %. During the exhaust stroke, the piston moves towards TDC, which further pushes the mass of gases in cylinder to leave the engine. At 360 °CA, the mass of gases residing in the clearance volume, which is termed as the residual gas, will be mixed with the fresh intake charge in the subsequent cycle.

6. CONCLUSIONS

Modelling of engine in-cylinder thermodynamic under high values of ignition retard (HVIR) was conducted with the objective of improving exhaust gas availability for heating TWC so that rapid catalyst lightoff can be achieved at engine cold-start. Emphases of this paper were on improving the predictive capability of the engine model under extreme spark retard where commonly used Wiebe function describing the fuel burning rate is not suitable. Modified Wiebe function was used in conjunction with an empirical correlation for cylinder pressure variation during the mass blowdown process, which occurs between the exhaust valve opened and bottom-dead-centre. In addition, the complicated mass blowdown process across the exhaust valves was simplified by two processes: (i) isentropic expansion from the cylinder pressure to the constant exhaust manifold pressure, and (ii) constant pressure throttling which gives rise to increased exhaust gas temperature due to the recovery of kinetic energy. Simulated results show that the model is able to reproduce the cylinder pressure reasonably well with capability of determining the cylinder temperature and trapped mass at exhaust valves opened, which are crucial for determining the increase in enthalpy, by HVIR, sufficient for heating the TWC within a defined time frame.

REFERENCES

[1] Zhu J., Chan S.H., An approach for rapid automotive catalyst lightoff by high values of ignition retard, J. Inst. Energy 69 (1996) 167–173.

[2] Ashley C., Techniques for future emission control at Bosch, Automotive Engineer 21 (1) (1996) 18.

[3] Heywood J.B., Motor vehicle emissions control: Past achievements, future prospects, IMechE 1997 George Stephenson Lecture, 6 November 1997, Singapore.

[4] Ferguson C.R., Internal Combustion Engines—Applied Thermosciences, Wiley, 1986.

[5] Olikara C., Borman G., A computer program for calculating properties of equilibrium combustion products with some applications on IC engines, SAE Paper 750468, 1975.

[6] Heywood J.B., Engine Combustion Modelling—An Overview from Combustion Modelling in Reciprocating Engines, Plenum Press, 1980.

[7] Woschni G., An universally applicable equation for the instantaneous heat transfer coefficient in the internal combustion engines, SAE Paper 670931, 1967.

[8] Woodward J.B., A second-law analysis of air-standard diesel-turbocharger-bottoming cycles, in: Proc. Instn. Mech. Engrs., Part D, J. Automobile Engineering 207 (1993) 107–114.

[9] Woodward J.B., Air-standard modelling for closed-cycle diesel engines, in: Proc. Instn. Mech. Engrs., Part D, J. Automobile Engineering 209 (1995) 115–123.

[10] Wu K.C., Hochgreb S., Numerical simulation of post-flame oxidation of hydrocarbons in spark ignition engines, SAE Paper 970886, 1997.

[11] Heywood J.B., Internal Combustion Engine Fundamental, Automotive Technology Series, McGraw-Hill, 1998.